NEUROSCIENCE

Somatostatin enhances visual processing and perception by suppressing excitatory inputs to parvalbumin-positive interneurons in V1

You-Hyang Song[1]*, Yang-Sun Hwang[1]*, Kwansoo Kim[1]*, Hyoung-Ro Lee[2]*, Jae-Hyun Kim[1], Catherine Maclachlan[3], Anaelle Dubois[3], Min Whan Jung[4], Carl C. H. Petersen[5], Graham Knott[3], Suk-Ho Lee[2], Seung-Hee Lee[1†]

Somatostatin (SST) is a neuropeptide expressed in a major subtype of GABAergic interneurons in the cortex. Despite abundant expression of SST and its receptors, their modulatory function in cortical processing remains unclear. Here, we found that SST application in the primary visual cortex (V1) improves visual discrimination in freely moving mice and enhances orientation selectivity of V1 neurons. We also found that SST reduced excitatory synaptic transmission to parvalbumin-positive (PV^+) fast-spiking interneurons but not to regular-spiking neurons. Last, using serial block-face scanning electron microscopy (SBEM), we found that axons of SST^+ neurons in V1 often contact other axons that exhibit excitatory synapses onto the soma and proximal dendrites of the PV^+ neuron. Collectively, our results demonstrate that the neuropeptide SST improves visual perception by enhancing visual gain of V1 neurons via a reduction in excitatory synaptic transmission to PV^+ inhibitory neurons.

INTRODUCTION

Somatostatin (SST) was initially identified as a secretory peptide that inhibits the release of pituitary growth hormone in the hypothalamus (*1*). Later, SST was found in a subset of GABAergic interneurons in the cerebral cortex, where it is expressed as a 14–amino acid peptide (*2*). Recent studies have identified the unique roles of SST-positive (SST^+) GABAergic neurons in cortical processing, mainly via dendritic inhibition (*3*–*5*). SST^+ neurons not only release γ-aminobutyric acid (GABA) but also have a strong potential of releasing the neuropeptide SST upon activation (*6*, *7*), but the exact effect of SST exerting peptidergic modulation in the cortex is yet to be fully elucidated. Reduction of SST expression has been proposed as a hallmark of various pathological conditions such as Alzheimer's disease (*8*), schizophrenia (*9*), epilepsy (*10*), and depression (*11*). However, it is still unclear whether SST released from the GABAergic neurons has a critical role in maintaining the cognitive function of the brain, especially in the cortex where the SST is expressed abundantly.

There are five subtypes of SST receptors (SSTRs), and all of them are G protein–coupled receptors that suppress neuronal activity and excitability (*7*). The inhibitory effect of SST signaling reduces excitatory synaptic transmission in many brain regions including the cerebral cortex (*12*). However, the net modulatory effect of SST is not just a simple inhibition within a complex cortical network, as SST can decrease not only excitatory but also inhibitory synaptic transmission via suppressing GABA release in GABAergic neurons (*13*, *14*). When SST is delivered to the cortex together with acetylcholine, it can even increase neuronal excitability (*15*). Furthermore, the modulatory effect of SST can vary depending on the receptor expression and the concentration of SST within the local circuits (*16*). Previous studies have examined the expression pattern of different subtypes of SSTRs in the cortex (*17*), but the subcellular localization of SSTRs in various types of cortical cells including excitatory, inhibitory, or non-neuronal cells are not clearly understood yet.

SST^+ neurons in the cortex are known to exert dendritic inhibition on pyramidal neurons via GABAergic transmission. SST^+ neurons can also disinhibit excitatory neurons via inhibiting other GABAergic neurons such as parvalbumin-positive (PV^+) neurons (*18*). Both SST^+ and PV^+ interneurons are interconnected with the excitatory pyramidal neurons in the cortical network to shape the feature selectivity of V1 neurons. Previous reports have shown that optogenetic activation of PV^+ or SST^+ neurons causes distinct effects on the orientation selectivity of V1 neurons in mice (*19*–*21*). The follow-up study showed that the duration of light stimuli relative to visual stimuli on the same population of inhibitory neurons gave different effects on the orientation selectivity of V1 neurons (*22*). All these studies used optogenetic tools to directly activate subtypes of GABAergic neurons and increase their inhibitory effects in cortical circuits. In the case of SST^+ neurons, however, not only the GABA but also the neuropeptide SST can be released upon the repetitive activation, as the dense-core vesicles (DCVs) containing peptides typically require a high level of neuronal activity to be released compared to the clear synaptic vesicles containing low–molecular weight neurotransmitters (*23*).

We therefore examined whether the activation of SSTRs by SST is involved in modulating visual processing in the cortex. To understand SST release independent of GABAergic transmission, we delivered purified SST peptides into the mouse V1 in vivo. We found that SST treatment and activation of SSTRs in V1 improves visual perception of mice performing an orientation discrimination task. Furthermore, SST treatment enhanced orientation selectivity of V1 neurons in vivo and reduced excitatory synaptic transmission to PV^+ interneurons in acute V1 slices. Last, we traced the axons of SST^+ neurons within intact V1 circuits using serial block-face scanning electron microscopy (SBEM) to examine their ultrastructure

[1]Department of Biological Sciences, KAIST, Daejeon 34141, Republic of Korea. [2]Department of Physiology, Seoul National University College of Medicine, Seoul, Republic of Korea. [3]Biological Electron Microscopy Facility, Centre of Electron Microscopy, École Polytechnique Fédérale de Lausanne (EPFL), Lausanne, Switzerland. [4]Center for Synaptic Brain Dysfunctions, Institute for Basic Science and Department of Biological Sciences, KAIST, Daejeon 34141, Republic of Korea. [5]Brain Mind Institute, Faculty of Life Sciences, École Polytechnique Fédérale de Lausanne (EPFL), Lausanne, Switzerland.
*These authors contributed equally to this work.
†Corresponding author. Email: shlee1@kaist.ac.kr

and wiring patterns. Vesicular clusters in the axons of SST^+ neurons often make contact with excitatory axons innervating the cell body and proximal dendrites of PV^+ interneurons. Our results demonstrate that the neuropeptide SST has a unique role in modulating visual gain in V1 microcircuits via preferential suppression of excitatory synaptic transmission onto the perisoma of PV^+ neurons.

RESULTS

Activation of SSTRs in the V1 improves visual perception in freely moving mice

To examine whether SST modulates visual perception, we devised a perceptual task for freely moving mice in the T-maze system (Fig. 1A). In this task, mice need to discriminate vertically oriented grating bars drifting rightward and the horizontally oriented bars drifting upward by associating water rewards on the right and the left choices, respectively. Individual mice showed steady learning, and we trained them until the discrimination performance reached >70% correct choices at the speed of executing two trials per 1 min (fig. S1, A and B). Well-learned mice showed equal levels of correct rates in choosing left or right water ports (fig. S1C). The individual animal showed variations in the learning speed (4 to 32 days) and the performance speed, but there was no correlation between them (fig. S1D). When we presented the lower-contrast visual stimuli to these mice, correct rates decreased gradually as decrement of perceptual ability (Fig. 1B). We then injected the purified SST (750 nl, 0.61 mM) or the cyclo-SST (c-SST; 750 nl, 0.64 mM), a modified peptide that is known as a blocker of SSTRs, into the V1 bilaterally (Fig. 1, C and D). We estimated the spread of peptides by injecting the same volume and concentration of fluorescein isothiocyanate (FITC)–conjugated SST into the V1 and imaging the fluorescence signal across the brain section covering the V1. We found that the injected peptide fluorescence signal covered ~26.4% of the V1 (fig. S1, E and F), indicating that the final concentration of the injected peptides was diluted up to 0.35 to 0.37 mM within the V1. Mice injected with SST showed a significant enhancement of perceptual behaviors, whereas c-SST–injected mice showed a significant reduction in visual discriminability of task-engaged mice (Fig. 1, E to G and L and fig. S1, G to J). We next examined whether the whole-brain treatment of SST or c-SST has a similar effect on mouse perceptual behaviors. When we infused the same concentration and volume of peptides into the ventricle, which is estimated to elevate cortical peptide concentration to 26 to 27 μM, mice also showed clear bidirectional changes in their perceptual behaviors (Fig. 1, H to K and M, and fig. S1K). Collectively, our data show that both local infusion and systemic injection of SST in the brain have a significant effect on improving visual perception of freely moving mice potentially via modulating brain circuits in vivo.

Not only the SST but also the cortistatin (CST), a member of SST peptide family expressed in a subset of cortical neurons (figs. S2A and S3), bind to and activate the SSTRs (*24*). When we infused CST into the V1, we also observed a similar enhancement of visual performance in behaving mice (fig. S2, B to D). Thus, activation or inactivation of SSTRs in the cortex enhances or disrupts visual perception in behaving mice, and SSTR signaling pathway in the cortex is critical for maintaining the perceptual ability in mice. We next wondered what types of SSTRs are expressed in the V1. We used single-cell RNA-sequencing data that are accessible in the Allen Brain Atlas data portal (*25*). Distinct types of V1 neurons showed different levels of five subtypes of SSTRs (fig. S3). Among the five types, the SSTR2 is the most abundant subtype of SSTRs expressed in the V1 and particularly enriched in the excitatory neurons of deeper layers (below layer 4) and a subset of inhibitory neurons that are developmentally originated from the caudal ganglionic eminence (CGE) (fig. S3, A and B) (*25*). PV^+ interneurons, compared with other cell types in the V1, express very little amount of SSTRs (fig. S3B). Thus, it is highly plausible that the effect of SST in the V1 is mostly due to the modulation of deep-layer excitatory neurons.

SST treatment enhances orientation selectivity of V1 neurons

We further examined how SST modulates V1 cortical processing in vivo. We first measured the orientation selectivity of V1 neurons by in vivo multichannel recording after treatment of SST or vehicle [phosphate-buffered saline (PBS)] into the cortex of anesthetized mice (Fig. 2, A and B). Consistent with the effect of SST treatment on perceptual behaviors, SST treatment improved the orientation selectivity of V1 neurons across the visual contrasts (Fig. 2, C to F). The increase of orientation selectivity index (OSI) was higher in neurons located near layers 4 to 5 defined by the depth of recording sites (Fig. 2, C, E, and F), suggesting that neural circuit modulation by SST has more influences on the deeper-layer cortical neurons.

We next examined whether SST treatment alters firing rates of V1 neurons (Fig. 2, H and I). When we analyzed waveform widths of isolated single units recorded in V1 and compared the fast-spiking (FS) neurons with the regular-spiking (RS) neurons, SST treatment significantly suppressed visual responses of FS neurons while enhancing those of RS neurons (Fig. 2, G to I). When we plotted their firing rates at different orientations, FS neurons significantly decreased their firing rates at all orientations (fig. S4A). On the contrary, RS neurons more strongly increased their firing rates at their preferred orientations (fig. S4B). Overall, V1 neurons more strongly increased firing rates at the preferred orientations, resulting in enhanced orientation selectivity and visual gain (fig. S4, C and D). Spontaneous firing rates of both FS neurons and RS neurons did not change significantly upon SST treatment, although there was a clear tendency of changes similar to the evoked responses (fig. S4E). FS neurons in the cortex are mostly inhibitory neurons, especially expressing the calcium-binding protein PV, and reduced activity of PV^+ neurons can increase the visual gain and orientation selectivity of V1 neurons (*20*). Our data suggest that the reduced visual responses of FS neurons by SST treatment caused the enhancement of orientation selectivity of V1 neurons in vivo.

SST treatment reduces excitatory synaptic transmission to the PV^+ neurons

We next wondered how the FS interneurons, potentially the PV^+ neurons, showed reduced activity upon the SST treatment without expression of SSTRs (fig. S3B). To understand this, we first performed in vitro patch-clamp recordings on FS and RS neurons in V1 slices and measured excitatory synaptic inputs to them while applying SST into the bath (Fig. 3A). We observed a significant reduction in the number of spontaneous excitatory postsynaptic currents (sEPSC frequency) in FS neurons but not in RS neurons (Fig. 3, B and C). On the other hand, the resting membrane potential of these neurons was not altered by the SST treatment (fig. S5A), suggesting that intrinsic membrane properties were not affected by the SST treatment. We next tested whether the high-frequency,

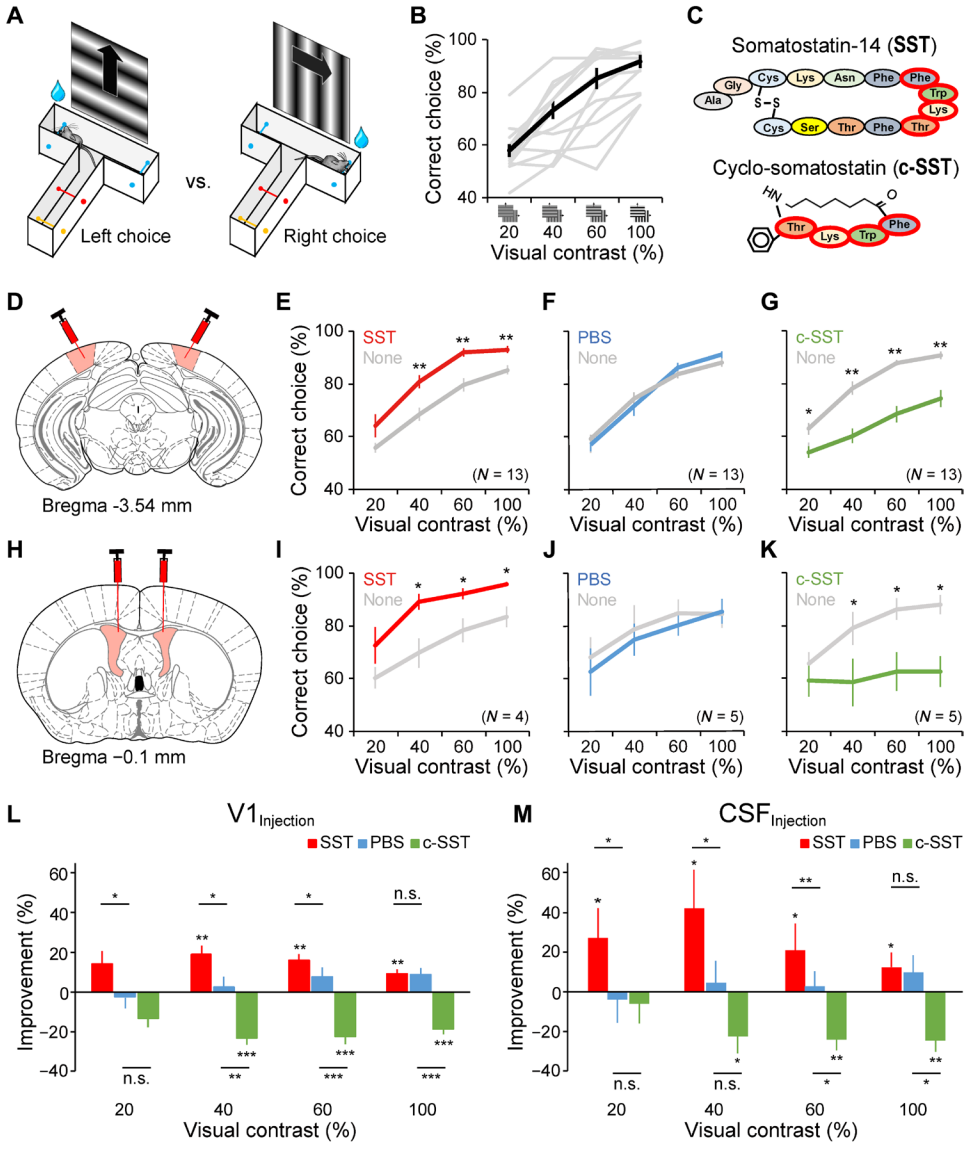

Fig. 1. Effects of SST and cyclo-SST injections on the visual discrimination performance of mice. (**A**) Schematic of the visual orientation discrimination task for freely moving mice in the T-maze. Lines are indicating infrared light beams that detect whether the beam braking happens via the passage of a mouse. Yellow, task-starting point; red, stimulus onset point; blue, choice detection point. (**B**) Contrast-dependent discrimination performance of 13 mice after learning. Gray lines, performance of individual mice; black line, average performance; means ± SEM (56.77 ± 2.27, 68.7 ± 3.45, 78.99 ± 3.89, and 85.72 ± 2.27). (**C**) Chemical structures of the injected peptides; SST-14 (SST) and cyclo-SST (c-SST). Red circles indicate the receptor-binding site of the peptides (F-W-K-T). (**D**) Schematic of bilateral injection of peptides into the mouse V1 (red). (**E** to **G**) The average performance of 13 mice in contrast-dependent visual discrimination with SST (E; red line), phosphate-buffered saline (PBS) (F; blue line), and c-SST (G; green line) injections. Data show means ± SEM (None versus SST, 55.79 ± 2.06 versus 64.18 ± 4.29, 68.53 ± 3.26 versus 80.84 ± 2.50, 79.57 ± 2.47 versus 91.94 ± 1.63, 85.22 ± 1.87 versus 92.92 ± 1.43; None versus PBS, 59.10 ± 1.76 versus 56.98 ± 2.54, 74.34 ± 2.61 versus 71.48 ± 3.56, 83.52 ± 1.48 versus 85.96 ± 2.01, 87.98 ± 1.54 versus 90.98 ± 1.34; None versus c-SST, 62.82 ± 2.28 versus 54.04 ± 2.12, 78.22 ± 2.51 versus 60.12 ± 2.73, 87.80 ± 1.06 versus 68.35 ± 3.14, 90.57 ± 1.46 versus 74.30 ± 3.13). Wilcoxon signed-rank test with Bonferroni correction (*P < 0.05, **P < 0.01). (**H**) Schematic of bilateral injections of peptides into the mouse lateral ventricle. (**I** to **K**) Average visual performance to four different contrasts of visual stimuli after injections of SST (I; red line), PBS (J; blue line), and c-SST (K; green line) into the cerebrospinal fluid (CSF). Data show means ± SEM (None versus SST, 59.19 ± 4.13 versus 72.30 ± 7.04, 69.28 ± 5.96 versus 89.06 ± 3.11, 78.63 ± 4.63 versus 92.17 ± 2.13, 83.22 ± 3.59 versus 95.79 ± 0.85; None versus PBS, 69.25 ± 7.42 versus 62.32 ± 9.00, 78.32 ± 9.10 versus 74.47 ± 6.10, 84.63 ± 5.83 versus 80.23 ± 4.02, 84.19 ± 5.85 versus 85.42 ± 4.66; None versus c-SST, 63.26 ± 4.39 versus 59.58 ± 6.10, 75.21 ± 6.54 versus 58.79 ± 9.03, 82.38 ± 5.34 versus 62.90 ± 7.25, 84.05 ± 5.02 versus 62.92 ± 5.87). Wilcoxon signed-rank test; *P < 0.05 with Bonferroni correction. (**L** and **M**) Percent improvements at each contrast by the peptide injection into V1 (L; $V1_{Injection}$, SST, 14.81 ± 6.03, 19.89 ± 4.56, 16.57 ± 3.34, 9.49 ± 2.37; PBS, −1.92 ± 5.35, 2.47 ± 5.75, 8.04 ± 3.67, 9.07 ± 2.91; c-SST, −12.79 ± 4.40, −22.76 ± 3.35, −22.09 ± 3.63, −18.19 ± 2.66) and CSF (M; $CSF_{Injection}$, SST, 24.64 ± 13.60, 38.09 ± 23.10, 18.91 ± 12.28, 12.57 ± 5.91; PBS, −3.87 ± 12.16, 4.16 ± 10.04, 2.23 ± 7.15, 8.89 ± 7.84; c-SST, −5.14 ± 9.90, −22.26 ± 8.97, −23.77 ± 5.50, −24.41 ± 5.49). Red, SST injection; blue, PBS injection; green, c-SST injection. Data show means ± SEM. Paired t test for (L) and Wilcoxon signed-rank test for (M); *P < 0.05, **P < 0.01 with Bonferroni correction. n.s., not significant.

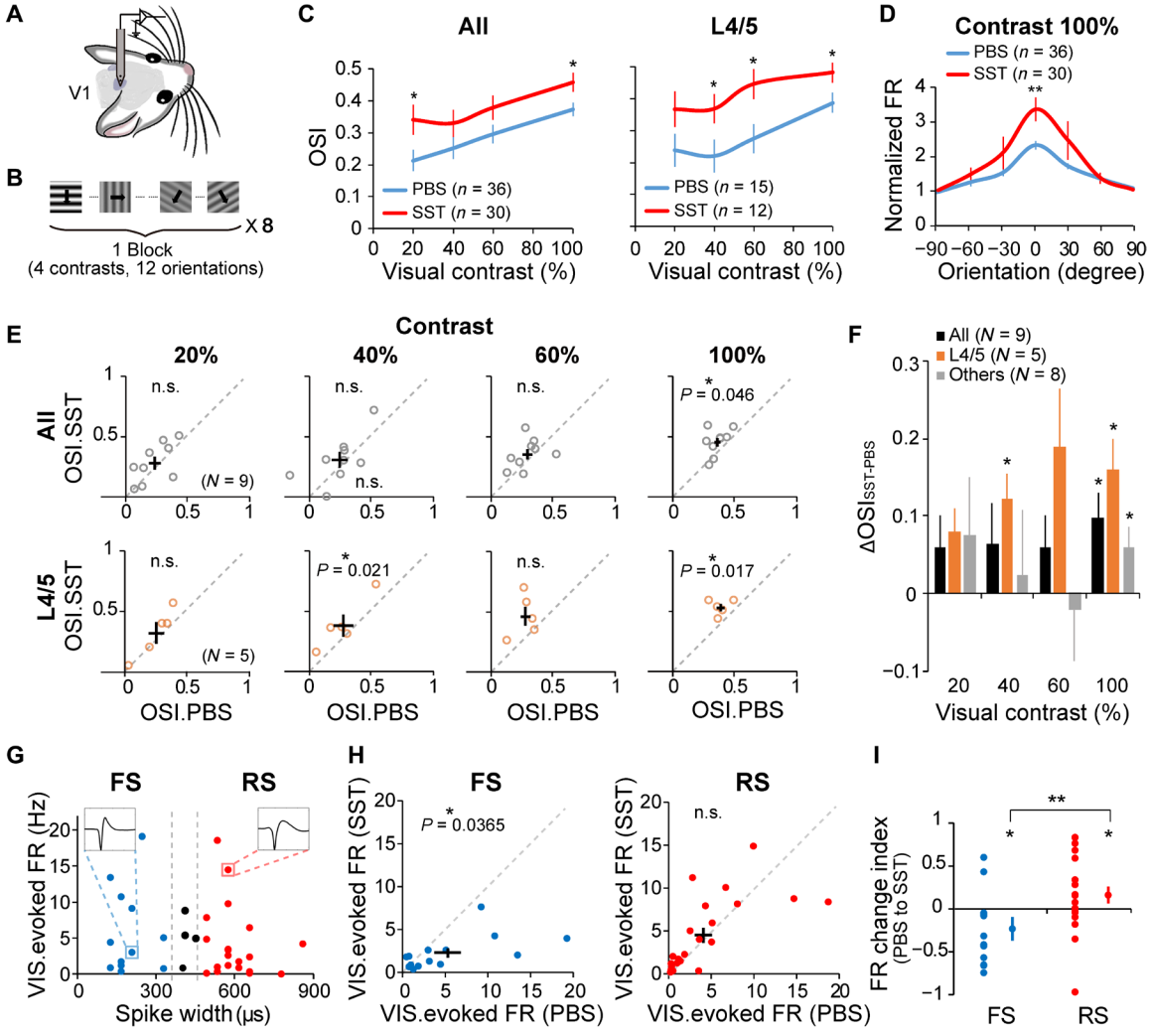

Fig. 2. SST increases the orientation selectivity and visual-evoked activity in the V1 of anesthetized mice. (**A**) Schematic for in vivo recordings in the V1. (**B**) Visual stimuli used for measuring orientation selectivity of V1 neurons. (**C**) The mean OSI of all units recorded throughout the layers of V1 (All: blue, PBS, $n = 36$; red, SST, $n = 30$) and the cells located in layers 4 to 5 (450 to 525 μm in depth from the pia; L4/5: blue, PBS, $n = 15$; red, SST, $n = 12$). Data show means ± SEM (All: PBS, 0.21 ± 0.03, 0.25 ± 0.03, 0.30 ± 0.03, 0.37 ± 0.02 and SST, 0.34 ± 0.05, 0.33 ± 0.04, 0.38 ± 0.04, 0.46 ± 0.03; L4/5: PBS, 0.24 ± 0.05, 0.22 ± 0.05, 0.27 ± 0.05, 0.39 ± 0.03 and SST, 0.37 ± 0.06, 0.37 ± 0.05, 0.45 ± 0.05, 0.48 ± 0.03). Unpaired *t* test with Bonferroni correction (*$P < 0.05$; All: $P = 0.026$, 0.150, 0.086, and 0.023; L4/5: $P = 0.097$, 0.038, 0.015, and 0.043). (**D**) Average of normalized firing rates (FR) at 100% contrast drifting gratings across orientations. "0" indicates the preferred orientation (PBS, $n = 36$; SST, $n = 30$). Vertical lines, means ± SEM (PBS, 0.95 ± 0.02, 1.23 ± 0.12, 1.51 ± 0.11, 2.31 ± 0.12, 1.70 ± 0.09, 1.33 ± 0.08, 1.05 ± 0.02; SST, 0.99 ± 0.04, 1.46 ± 0.19, 2.10 ± 0.48, 3.36 ± 0.36, 2.46 ± 0.56, 1.35 ± 0.15, 1.01 ± 0.04). Unpaired *t* test; **$P < 0.01$ with Bonferroni correction. (**E**) Average OSIs of all V1 neurons (All: $N = 9$) and of the layer 4/5 neurons (L4/5: $N = 5$) with PBS and SST treatment. Open circles, individual mice; crosses, means ± SEM (All: PBS, 0.22 ± 0.05, 0.24 ± 0.06, 0.29 ± 0.04, 0.36 ± 0.02 and SST, 0.28 ± 0.05, 0.31 ± 0.07, 0.35 ± 0.04, 0.45 ± 0.04; L4/5: PBS, 0.24 ± 0.06, 0.26 ± 0.08, 0.27 ± 0.04, 0.38 ± 0.03 and SST, 0.32 ± 0.09, 0.38 ± 0.09, 0.46 ± 0.08, 0.54 ± 0.03). Paired *t* test (*$P < 0.05$; All: $P = 0.190$, 0.268, 0.145, and 0.046; L4/5: $P = 0.063$, 0.021, 0.066, and 0.017). (**F**) Differences between the OSIs measured in the same animal with SST and PBS treatments at different visual contrasts. Black bars, averages of All V1 neurons ($n = 9$ mice); orange bars, averages of L4/5 neurons ($n = 5$ mice); gray bars, other V1 neurons excluding L4 neurons ($n = 6$ mice). Bars, means ± SEM (All: 0.06 ± 0.04, 0.06 ± 0.05, 0.06 ± 0.04, 0.10 ± 0.03; L4/5: 0.08 ± 0.03, 0.12 ± 0.03, 0.19 ± 0.08, 0.16 ± 0.04; Others: 0.08 ± 0.06, 0.02 ± 0.05, −0.02 ± 0.04, 0.07 ± 0.03). Paired *t* test with Bonferroni correction (*$P < 0.05$; All: $P = 0.197$, 0.260, 0.210, and 0.022; L4/5: $P = 0.0623$, 0.021, 0.066, and 0.017; V1, $P = 0.113$, 0.331, 0.953, and 0.033). (**G**) Classification of the recorded cells as FS (blue dots) and RS (red dots) cells. Cells with spike widths less than 350 μs were classified as "FS" cells, and those with more than 450-μs widths were classified as "RS" cells (*39*, *40*). Insets, waveforms of example cells. (**H**) Comparison of visual-evoked firing rates of FS (left, blue dots, $n = 14$) and RS (right, red dots, $n = 24$) cells with the PBS and the SST treatments. Crosses, means ± SEM of all cells (FS: PBS, 5.33 ± 1.54 and SST, 2.31 ± 0.53; RS: PBS, 4.00 ± 1.01 and SST, 4.49 ± 0.88); Wilcoxon signed-rank test (*$P < 0.05$; FS: $P = 0.036$; RS: 0.064). (**I**) Firing-rate change index (PBS to SST) in the visually evoked activity of FS (blue dots) and RS (red dots) cells. Blue, FS cells; red, RS cells; dots and vertical lines, means ± SEM (FS, −0.24 ± 0.11; RS, 0.16 ± 0.08). Wilcoxon signed-rank test for zero comparison and Mann-Whitney *U* test for FS-RS comparison (*$P < 0.05$, **$P < 0.01$; FS: $P = 0.041$; RS: 0.046).

repetitive activation of SST^+ neurons induces the same effect on FS neurons by endogenous release of SST in the V1 slice. We labeled SST^+ neurons with hChR2(ETTC)-tdTomato and optogenetically stimulated them with a train of light pulses (40 Hz for 1 s) that was repeated 16 times (intertrain interval; 2.5 s) (fig. S6, A and B; see Materials and Methods). Meanwhile, we measured sEPSCs in FS and RS neurons before and after the light stimulation (Fig. 3D). We incubated the V1 slice with GABA type A ($GABA_A$) and $GABA_B$

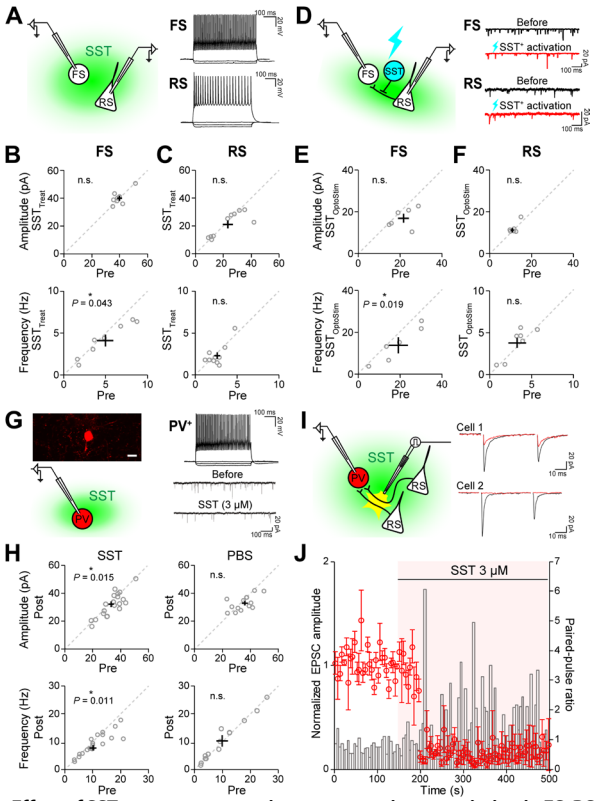

Fig. 3. Effect of SST treatment on excitatory synaptic transmission in FS, RS, and PV$^+$ neurons. (**A**) Left: Schematic for SST treatment on V1 slice with whole-cell patch-clamp recording of RS and FS cells. Right: Example traces of spiking activity for FS (upper panel) and RS cells (lower panel). Horizontal and vertical scale bars indicate time (ms) and membrane potential (mV). (**B**) Scatter plots representing sEPSC amplitude (upper panel) and frequency (lower panel) of FS cells before (Pre) and after SST treatment (SST_{Treat}; $n = 8$). Black lines, means ± SEM (Amplitude: Pre, 39.92 ± 1.85 and SST, 39.95 ± 1.81; Frequency: Pre, 4.95 ± 0.98 and SST, 4.13 ± 0.72); Paired *t* test (*$P < 0.05$). (**C**) Same as (B), but for RS cells ($n = 10$) (Amplitude: Pre, 23.20 ± 3.60 and SST, 21.18 ± 2.79; Frequency: Pre, 2.67 ± 0.33 and SST, 2.34 ± 0.40). (**D**) Left: Schematic for optogenetic activation of SST$^+$ interneurons in the V1 slice during whole-cell patch-clamp recording of RS and FS cells. Thunder indicates the blue light stimulation to activate SST$^+$ neurons. Right: Example traces of sEPSCs measured in an FS cell (two upper panels) and an RS cell (two lower panels) before and after activation of SST$^+$ neurons. (**E**) Scatter sEPSC amplitude (upper panel) and frequency (lower panel) of FS cells before (Pre) and after activation of SST$^+$ neurons ($SST_{OptoStim}$; $n = 6$). Bars, mean ± SEM (Amplitude: 21.49 ± 2.52 and 16.98 ± 2.14; Frequency: 18.86 ± 4.52 and 13.64 ± 3.79 for Pre and SST$^+$ activation condition); Paired *t* test (*$P < 0.05$). (**F**) Same as (E), but for RS cells ($n = 7$) (Amplitude: Pre, 11.17 ± 0.79 and SST, 11.11 ± 1.04; Frequency: Pre, 3.23 ± 0.59 and SST, 3.48 ± 0.71). (**G**) Left: The representative image of a PV$^+$ neuron labeled with the red-fluorescent protein (tdTomato; scale bar, 10 μm) (upper panel) and schematic for SST treatment onto V1 slice with whole-cell patch-clamp recording of PV$^+$ neurons (lower panel). Right: Example traces of spiking activity (upper panel) and sEPSCs (lower panel) measured in a PV$^+$ neuron before and after SST treatment (3 μM). (**H**) Scatter plots representing sEPSC amplitude (upper panel) and frequency (lower panel) of PV$^+$ cells before and after SST (left) or PBS (right) treatment (SST, $n = 20$; PBS, $n = 14$) (Amplitude: SST, Pre, 34.54 ± 1.82, Post, 31.75 ± 1.93, PBS, Pre, 35.80 ± 2.27, Post, 33.06 ± 1.57; Frequency: SST, 9.97 ± 1.28, Post, 8.21 ± 0.98, PBS, Pre, 10.06 ± 2.01, Post, 10.12 ± 2.00). Paired *t* test (*$P < 0.05$). (**I**) Left: Schematic for SST treatment onto V1 slice with whole-cell patch-clamp recording of a PV$^+$ neuron during paired-pulse electrical stimulations. Right: Two example traces of eEPSCs in PV$^+$ neurons before (black line) and after SST treatment (red line). (**J**) Normalized eEPSC amplitude (red open circles and lines, means ± SEM) and paired-pulse ratio (black open bars) before and after SST treatment. Horizontal bar and red-shaded box indicate the SST treatment period.

receptor antagonists to block GABAergic transmission. Consistent with the SST treatment condition, sEPSC frequency decreased in FS neurons, but not in RS neurons (Fig. 3, E and F).

To tell whether the SST modulation effect was specific to the PV$^+$ neurons, we next performed targeted patch-clamp recordings on the PV$^+$ neurons in the V1 slices of the PV::tdTomato mice (Fig. 3G). Similar to the results from FS neurons, SST treatment, but not the vehicle treatment, significantly reduced the amplitude and frequency of EPSCs in PV$^+$ neurons (Fig. 3, G and H). Both the resting membrane potential and the rheobase of PV$^+$ neurons were not changed by the SST treatment (fig. S5B), indicating that SST modulates excitatory synaptic transmission to the PV$^+$ neurons without altering the intrinsic membrane properties of PV$^+$ neurons. The results also suggest that the SST exerts presynaptic modulation of the excitatory synaptic transmission since SSTRs are not expressed in PV$^+$ neurons (fig. S3B). To further confirm the presynaptic effect of SST on excitatory inputs to PV$^+$ neurons, we measured evoked EPSCs (eEPSCs) in PV$^+$ neurons by applying electrical stimulation and directly driving excitatory inputs to the recorded neurons (Fig. 3I and fig. S6C). SST treatment significantly decreased eEPSC amplitude in a subset of stimulations given to PV$^+$ neurons (~36%; 4 of 11) (Fig. 3J and fig. S6, D and E). Furthermore, SST treatment clearly increased the paired-pulse ratio of eEPSC amplitudes (Fig. 3J). These data support the idea that SST suppresses and modulates the presynaptic release of excitatory neurotransmitters to PV$^+$ neurons in the V1. To sum up, the presynaptic modulation can decrease the visual responses of PV$^+$ neurons in V1 circuits and, in turn, increases visual gain and orientation selectivity of overall V1 neurons (Fig. 2). Therefore, the modulation potentially improves visual perception in behaving mice (Fig. 1).

SST$^+$ axons with vesicle clusters are apposed to the excitatory axons innervating perisoma of PV$^+$ neurons

So far, our results showed that the application of SST to the V1 has a specific modulatory effect on the excitatory synaptic transmission to the PV$^+$ neurons and visual processing in vivo. However, it was still unclear whether the specific circuit mediating this presynaptic modulation of the excitatory inputs to PV$^+$ neurons exists in V1 microcircuits in vivo. To unravel this, we performed the correlative light and electron microscopy (EM) by the SBEM to reconstruct the three-dimensional (3D) ultrastructure of SST$^+$ axons (labeled with green fluorescence) nearby the soma of a PV$^+$ neuron (labeled with red fluorescence) in the V1 samples obtained by crossing GIN and PV::tdTomato mice (Fig. 4, A and B, and movie S1; see Materials and Methods). In the brain samples of these mice, green fluorescent protein (GFP) is expressed in a subset of SST$^+$ neurons, and tdTomato is expressed in the PV$^+$ neurons.

In the obtained EM image stacks, we first identified the soma and the initial dendritic segments of the red PV$^+$ as well as the ghost PV$^-$ neurons and analyzed presynaptic excitatory and inhibitory synapses formed on those structures (Fig. 4B and movie S1). PV$^+$ neurons, compared with the PV$^-$ neurons, received more asymmetric synaptic inputs (typical type I synapses) on the perisoma (Fig. 4C). We then traced the axons of SST$^+$ neurons in the image stacks nearby the dendrites (movie S1). In places, we found that axons of SST$^+$ neurons were apposed to axons that made excitatory synapses on the perisoma of the PV$^+$ neuron (Fig. 4D). At this apposition were clusters of vesicles including dark-stained DCVs in the SST$^+$ axons (Fig. 4D). The PV$^-$ perisomatic dendrites received mostly inhibitory synaptic

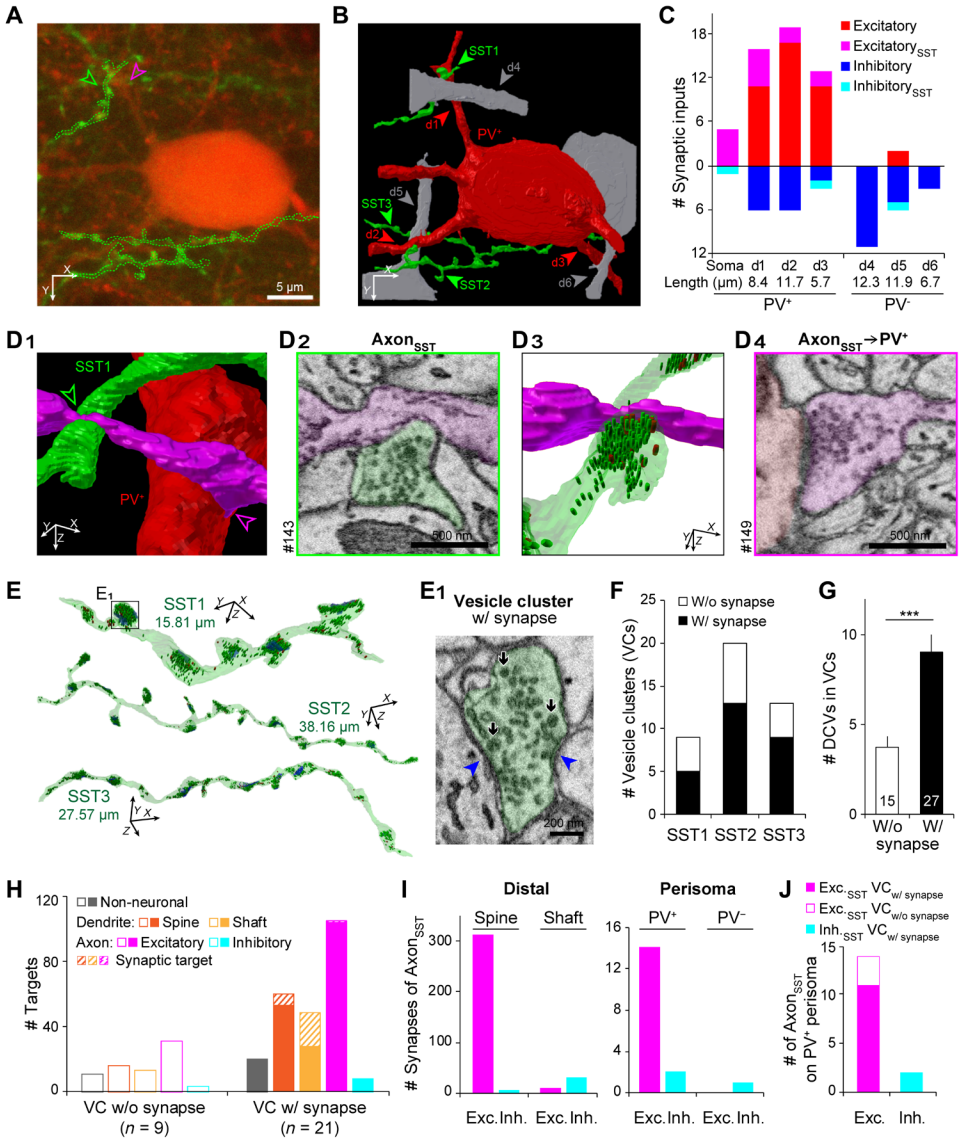

Fig. 4. PV$^+$ neurons receive perisomatic excitatory synaptic inputs that are innervated by axons of SST neurons. (**A**) The *z*-projection image of the red fluorescent PV$^+$ and the green fluorescent SST axons taken by a confocal microscope. Dotted green lines indicate three SST axons traced by the SBEM. Green and magenta arrows indicate the same regions shown in (D). (**B**) The 3D-reconstructed view of the PV$^+$ perisoma (red, PV$^+$) and the three SST axons (green, SST) shown in (A) together with the three PV$^-$ soma and proximal dendrites (gray). White arrows indicate the projection angle of the 3D view. (**C**) The number of synaptic inputs to the soma and the proximal dendrites of the PV$^+$ neuron (soma, d_1 to d_3, PV$^+$) and PV$^-$ neuron (d_4 to d_6, PV$^-$) in (B). Magenta and cyan indicate synapses made by axons contacting with SST axons. (**D$_1$**) The representative view of the SST axon (green), PV$^+$ dendrite (red) and excitatory axon (magenta) shown in (A). Green arrow indicates the contacting point of the SST axon with the excitatory axon making synapse on the proximal PV$^+$ dendrite (magenta arrow). (**D$_2$**) Axon$_{SST}$, a representative SEM image showing contact of SST axon (green) to the excitatory axon innervating PV$^+$ dendrite (magenta). (**D$_3$**) 3D-reconstructed view of the SST and excitatory axons shown in (D_2). Note the zoomed-in view of the vesicle cluster (VC) contains both synaptic vesicles (SVs; green) and DCVs (red). Black arrows, 3D projection angle. (**D$_4$**) Axon$_{SST}$ → PV$^+$, a representative SEM image showing excitatory axon making synapse on the proximal dendritic shaft of the PV$^+$ neuron (red). Note that the axon makes the type I excitatory synapse. Scale bars, 500 nm. Numbers on the left indicate the number of sections from SBEM image stacks. (**E**) 3D reconstruction of SST axons (light green) with VCs. Green dots, small SVs; red dots, DCVs; blue shades, type II inhibitory synapses; black arrows, the 3D projection angles of individual axons. Note that DCVs are always found in VCs. (**E$_1$**) Zoomed-in SEM image of a VC in the SST1 axon (green) boxed in (E). Note that the VC contains both DCVs (black arrows) and inhibitory synapses (blue arrows). (**F**) The number of VCs identified in SST axons (SST1-SST3). Open bar, VCs without synapse; closed bar, VCs with synapse. (**G**) The number of DCVs in VCs with (closed bar, 27 clusters; 9.00 ± 1.21) or without (open bar, 15 clusters; 4.00 ± 0.82) synapses. Data show means ± SEM (***$P < 0.001$). (**H**) The number of targets of SST axons with VCs with or without synapses. Note that there are five classes of targets: non-neuronal cells, dendritic spines, dendritic shafts, excitatory axons, and inhibitory axons. Combed bar, targets connected by type II synapses. (**I**) Synaptic targets of excitatory axons (magenta) and inhibitory axons (cyan) receiving SST axonal contacts. Postsynaptic targets within two synaptic boutons from the contacting point were counted. Bars indicate total number of postsynaptic targets. Note that the most targeted were the distal dendritic spines and the second most targeted was the PV$^+$ perisoma. (**J**) The number of axons contacted by SST axonal VCs and innervating the PV$^+$ perisoma. Closed bar, axons contacted by SST synaptic VCs; open bar, axons contacted by SST nonsynaptic VCs.

inputs (type II synapses), and the axons making inhibitory synapses on the PV^+ neuron or neighboring PV^- neurons show little interaction with the SST^+ axons (Fig. 4C).

We further examined the distribution of vesicles in the traced GFP^+ axons and contacting targets of these axons to understand the location of DCVs and presynaptic terminals along the axons of SST^+ neurons (Fig. 4E). There were distinct locations where vesicle clusters (VCs) are along the GFP^+ axons, and all of these VCs contained DCVs (Fig. 4E). More than 50% of VCs were presynaptic boutons that form inhibitory synapses preferentially on the dendritic shaft of spiny postsynaptic neurons (Fig. 4, E to H). There were more DCVs in the presynaptic VCs (Fig. 4G), suggesting that DCVs that potentially contain SST peptides in SST^+ neurons can be coreleased at the presynaptic bouton where GABAergic synaptic transmission occurs.

Axonal membranes of SST^+ neurons containing VCs made not only type II symmetric synaptic junctions to the postsynaptic targets (mostly dendritic shaft) for GABAergic synaptic transmission but also the membrane-to-membrane contacts with neighboring cells within the 3D space (Fig. $4D_3$). Since the DCVs can be released outside the active zones, we assumed that the cellular compartments apposed to the axonal membranes with VCs are the primary targets of DCVs released by the volume transmission. We thus identified all membrane contacts of SST^+ axonal membranes where DCVs were found in the VCs. The majority of membrane contacts of the SST^+ axonal VCs was the excitatory axons, even more than the dendritic spines or shafts (Fig. 4H). When we traced postsynaptic targets of these excitatory axons contacting SST^+ axons within <2 synapses from the contacting point, the most abundant target was the spines on the distal dendrites, and the second-most one was the perisoma of the PV^+ neuron (Fig. 4, I and J). Considering that perisomatic excitatory inputs are most influential in the generation of postsynaptic responses, our EM data demonstrate that axonal release of SST from the SST^+ neurons can preferentially and presynaptically modulate the excitatory synaptic transmission to the perisoma of PV^+ neurons in vivo (Fig. 4J). These data also support our findings on the modulatory effect of SST treatment on the V1 microcircuits.

DISCUSSION

In this study, we examined the modulatory function of SST in the V1 cortical circuits. We found that exogenous application of SST into the V1 caused suppression of excitatory synaptic transmission to the PV^+ neurons and reduced their visual responses, which led to the enhancement of orientation selectivity of V1 neurons and visual discriminability in mice. We have identified the ultrastructure of SST^+ axons that make direct membrane-to-membrane contacts with axons forming excitatory synapses on the PV^+ dendrites. Our study demonstrates a previously unknown circuit paradigm that the neuropeptide SST expressed in a subset of cortical interneurons has an important role in modulating cortical processing. We showed that activation of SSTRs in vivo is required for and further improves visual perception in the actively navigating animal, and these data strongly support the idea that SST can be therapeutically applicable as a drug to treat cognitive disorders with deficits in sensory perception and visual cognition such as Alzheimer's disease (*26*).

So far, most of the studies on cortical microcircuits consider the function of SST^+ neurons as GABAergic neurons exerting dendritic inhibition onto the principal neurons. In particular, artificial activation or inactivation of a subtype of GABAergic neurons with optogenetic techniques allowed researchers to isolate the function of distinct interneuron subtypes in complicated cortical circuits (*19*–*21*). However, GABAergic neurons in the cortex, including SST^+ interneurons, often express specific peptides as marker proteins, and these peptides can be coreleased with GABA into the cortical space when the neurons are strongly activated. Differences in the intensity and duration of photostimulation as well as sensory stimulation can induce different levels of activity in the peptide-expressing GABAergic neurons within cortical circuits, and it is plausible that certain conditions may promote the release of peptides more within cortical circuits and modulate cortical processing in different directions. Therefore, understanding the modulatory function of these peptides in cortical circuits is crucial to elucidate the genuine function of interneurons in the cortex.

Our study illustrates the unique role of SST in cortical circuits in vivo and suggests that the neuropeptide SST is critical and must be considered in studies using experimental techniques of manipulating and measuring the activity of SST^+ neurons in the cortex. Additional SST enhanced the visual discrimination performance while the SSTR blocker (c-SST) hampered the performance. To understand more specific function of SST and subtypes of SSTRs, it is required to test selective antagonists for SSTRs or use the CRISPR-Cas9 system to knock out SST/SSTR subtypes in vivo. Future studies are also necessary to unravel activity patterns of SST^+ neurons in vivo that induce GABA and SST releases from the same SST^+ neurons. Dissociating physiological mechanisms underlying SST versus GABA release from the same SST^+ neurons may provide an important scope on the intrinsic property of GABAergic interneurons that corelease neuropeptides in vivo. It will be also necessary to examine whether there is a selective change in the expression of SST compared to other GABAergic markers in pathological conditions to dissect disorders that are linked more specifically to the function of SST.

Although we found that SST presynaptically modulates excitatory inputs to the PV^+ interneurons by in vitro electrophysiology and provided evidence of these wiring patterns in vivo by 3D reconstruction of SST^+ axons with DCVs, we were not able to examine the subcellular localization of SSTRs and SST peptides in V1 circuits. The immuno-EM data have provided evidence of axo-axonic synapses formed by the SST^+ axons in the rat and monkey visual cortex (*27*), but this study did not identify the target of axons innervated by SST^+ axons. Early studies have shown that the SSTR2 is the major SSTR expressed in the cortex and depresses the activity of pyramidal neurons (*17*, *24*, *28*). Our analysis of recent single-cell RNA-sequencing data from Allen Brain Institute (*25*) also supports the idea that the SSTR2 is the major subtype of SSTRs expressed in the cortex and further showed that the SSTR2 is especially enriched in deep-layer excitatory neurons and interneurons developed from the CGE (fig. S3, A and B). Consistent with this, the development of specific antibodies against the SSTR2 revealed higher expression of the SSTR2 in deeper cortical layers (*29*, *30*), but the exact subcellular localization of the receptors is still controversial and not clearly understood yet (*31*). Not only the cortical neurons but also the thalamic afferents also express SSTRs (*32*). Although we still do not know which axonal projections express SSTRs in vivo, it is plausible that SST modulates feed-forward inputs to PV^+ neurons, which are mostly perisomatic, rather than feedback inputs on distal dendrites. Reduction in feed-forward inhibition may explain why the visual gain was increased by SST treatment. Regardless, our study revealed the 3D ultrastructure and connectivity of SST^+ axons nearby the PV^+ soma and gave us

critical insights on the wiring paradigm of SST^+ neurons in V1 microcircuits. New techniques combining less destructive immunostaining protocol with the correlative light EM may help to unravel the exact location where the SST peptides are released and bind in intact cortical circuits in vivo.

MATERIALS AND METHODS

Animal subjects

The Korea Advanced Institute of Science and Technology Institutional Animal Care and Use Committee (IACUC KA2016-23), the Seoul National University Institutional Animal Care and Use Committee (SNU-111104-5), and Swiss Federal Veterinary Office (VD1628) approved all experimental procedures for animal usage. For behavior and in vivo electrophysiology experiments, wild-type mice (C57/BL6J) in postnatal days 80 (P80) to 150 (P150) were used. For the whole-cell patch-clamp recordings of FS and RS neurons in V1, wild-type (B6;129PF2J; P15 to P40, Jackson Laboratories) mice were used. For patch-clamp recordings of PV^+ neurons, PV::tdTomato mice, descendants from PV-Cre mice [B6;129P2-Pvalb$^{(tm1(cre)Arbr)/J}$; Jackson Laboratories, stock no. 008069] crossed with the Ai14 mice [B6;129S6-Gt(ROSA)26Sor$^{(tm14(CAG-tdTomato)Hze)/J}$; Jackson Laboratories, stock no. 007908] were used to visualize and selectively target PV^+ neurons. For patch-clamp recording of FS and RS neurons with optogenetic activation of SST^+ neurons, SST-Cre [Sst$^{tm2.1(cre)Zjh/J}$, Jackson Laboratories, stock no. 013044] mice were used to visualize and selectively stimulate SST^+ neurons. For the 3D EM tracing, the descendants from GIN mice [FVB-Tg(GadGFP)45704Swn/J; Jackson Laboratories, stock no. 003718] crossed with PV::tdTomato mice (GINxPV::tdTomato) were used for labeling SST^+ neurons and PV^+ neurons with GFP and tdTomato, respectively.

Visual stimulation

Visual stimuli were generated with a PC containing an NVIDIA GeForce GT 730 graphics board using "Psychtoolbox" in MATLAB and presented with a TS-1508D LCD monitor (30.5 cm by 22.9 cm, 1024 × 768 pixels, 60-Hz refresh rate, 250 cd m^{-2} maximum luminance, gamma-corrected with custom software) located 14 cm from the left eye. For measuring orientation tuning of V1 neurons, full-field drifting gratings (20, 40, 60, and 100% contrast, 2 Hz, 0.04 cycles per degree, 2 s) were presented at 12 directions (separated by 30°) in a random sequence. A total of eight blocks were presented in each experiment. To measure orientation discriminability of behaving mice, we presented drifting gratings of the same contrast and spatiotemporal frequencies (100% contrast, 2 Hz, 0.04 cycles per degree, 2 s per trial).

Peptide solutions

The SST (S9129, Sigma-Aldrich) and CST (C5808, Sigma-Aldrich) were dissolved in the PBS at 1 mg/ml (0.61 and 0.58 mM, for each), and c-SST (3493, Tocris) at 0.5 mg/ml (0.64 mM). For measuring the spread of peptide, we synthesized fluorescent-conjugated SST (FITC-SST; K192251, Anygen) and dissolved it in the PBS at the same concentration with the SST used (0.61 mM). For in vitro patch-clamp recording, we diluted the high-concentration solution into the artificial cerebrospinal fluid (ACSF) to the desired concentration (see below).

Behavior paradigms

T-maze was custom-made with acrylic boards, and the board facing the monitor at the front side of the T-maze was built with the transparent acrylic board. The beam-break detection system was located at the four sites along the maze to detect the pass of subject mice (Fig. 1A). Mice were deprived of water before the training started. When mice choose the correct path in response to the visual stimuli, two valves connected to the water ports at the end of side corridors provided fresh water as a reward (5 to 7 μl at a time). Visual stimuli and water rewards were automatically given according to the beam-break signals by the custom software in LabVIEW (National Instruments). A total of 192 trials of equal numbers of the left and the right stimuli were presented in a random order in one session, and we quantified the correct choice (%) as follows

$$\text{Correct choice}(\%) = \text{total number of correct choice trials/total number of trials}$$

When mice reached 70% of correct choice rates, four contrasts (20, 40, 60, and 100%) of visual stimuli were randomly presented. Each type of stimuli was presented at equal ratio (48 trials per each contrast with an equal number of left and right stimuli), and the water reward was given to mice only when they choose the correct path.

Intracranial injection and histological confirmation

After the completion of learning, we injected the peptides into the V1 (bregma, −3.40 mm; lateral, 2.0 mm; depth, 0.50 mm) or into the ventricle (bregma, −0.1 mm; lateral, 0.9 mm; depth, 2.0 mm) bilaterally. For the intracranial injection, the small craniotomy (~0.5 mm in diameter) was made on the targeted sites of the mice under anesthesia with 1.5% isoflurane on 1 or 2 days before the injection. We fixed the head of a mildly anesthetized mouse in the stereotaxic frame and injected total 750 nl of the SST, the c-SST, or the CST into the V1 or the ventricle using the Nanoliter 2010 injector (WPI) at a speed of 50.6 nl/s for 5 min in each hemisphere. After finishing the injection, we put mice back to the home cage for 15 to 30 min until they fully recovered from the injection before the behavioral tests. To confirm the spread of the locally injected peptides, we injected 750 nl of FITC-SST into both hemispheres of V1 with same injection protocol as used for other peptides. After 15 min or 1 hour 15 min from the first injection, we euthanized the mice and collected the brain samples for the histology. For the whole-cell patch-clamp recordings with optogenetic stimulation of SST^+ neurons, we injected ~700 nl of AAV2/2-EF1α-DIO-hChR2(E123T/T159C)-eYFP into both hemispheres of V1. After 2 weeks of incubation, we euthanized the mice and performed in vitro experiment (see below).

For the histology, we perfused the animals with 0.1 M PBS followed by 4% paraformaldehyde (PFA, w/v) in 0.1 M PBS. After post-fixation of samples with 4% PFA, we placed them in 30% sucrose solution for 2 to 3 days in 4°C. Then, the samples were dehydrated and embedded in the optimal cutting temperature solution (Tissue-Tek, no. 4583) and frozen at −80°C. All the samples were sectioned at 40-μm thickness from −2.30 to −4.72 mm to the bregma covering most of V1 regions using a cryostat. After washing the slices with 1× PBS (three times) and mounting them in 4′,6-diamidino-2-phenylindole medium, we collected the images with a slide scanning microscope (Zeiss Axio Scan Z1) and measured the spread of fluorescent-conjugated peptides in the V1.

In vitro slice patch-clamp recordings

Mice between P15 and P55 were anesthetized with 1.5% isoflurane and transcardially perfused with the cold (0° to 4°C) slice cutting

solution (80 mM NaCl, 2.5 mM KCl, 1.3 mM NaH_2PO_4, 26 mM $NaHCO_3$, 4 mM $MgCl_2$, 0.5 mM $CaCl_2$, 20 mM D-glucose, 75 mM sucrose, and 0.5 mM sodium ascorbate; 315 mOsmol, pH 7.4, and saturated with 95% O_2/5% CO_2). The brains were then removed and sectioned into 300-μm coronal slices in the cutting solution by using a vibratome (Leica VT1200 S). Slices were incubated in the ACSF (119 mM NaCl, 2.5 mM KCl, 1.3 mM NaH_2PO_4, 26 mM $NaHCO_3$, 1.3 mM $MgCl_2$, 2.5 mM $CaCl_2$, 20 mM D-346 glucose, and 0.5 mM sodium ascorbate; 300 mOsmol, pH 7.4, and saturated with 95% O_2/5% CO_2) at 34°C, for at least 30 min before the recording. Recordings were performed in the same solution freshly given at a rate of around 3.0 ml/min. For whole-cell recordings, a K^+-based pipette solution that contains the following was used: 142 mM K^+-gluconate, 10 mM Hepes, 1 mM EGTA, 2.5 mM $MgCl_2$, 4 mM adenosine triphosphate–Mg, 0.3 mM guanosine triphosphate–Na, and 10 mM Na_2-phosphocreatine (295 mOsmol, pH 7.35).

Data were acquired at 20 kHz with an Axon MultiClamp 700B amplifier, an Axon Digidata 1550 Low-Noise Data Acquisition System (Molecular Devices), and an Integrated Patch Amplifier (Double IPA, Sutter Instrument) using the software Clampex 10.6 (Molecular Devices) and Igor7. Only the recording data showing the sustained series resistance below the 20 megohms were included. Data were analyzed using Clampfit 10.6 (for EPSCs) or Igor7 (for sEPSC, eEPSC, and paired-pulse ratio) or custom MATLAB codes (for intrinsic membrane properties of a cell). The resting membrane potential was recorded in the first minute right after the rupture. The rheobase and the membrane resistance were calculated by injecting 500-ms current, in a 30-pA step, from −60 to at least 240 pA, until at least 8 APs are observed in one current injection. sEPSCs were collected at the holding potential of −70 mV for at least 3 min. The peak amplitudes and the frequency of the peaks were calculated before and after the SST or the vehicle treatments. EPSCs were recorded at the whole-cell patch recordings on tdTomato$^+$ neurons in L2/3 of V1 at a holding potential of −70 mV (reversal potential for Cl^- = −70 mV). EPSCs were evoked by paired-pulse electrical stimulation (interpulse interval = 50 ms) using a monopolar glass electrode (4 to 8 V for 0.1 ms) filled with ACSF (pore resistance approximately 2 to 3 MOhm) positioned in L2/3. The SST stock solution in the PBS was diluted at 3 μM in ACSF. The brain slices were incubated in the diluted solution for 3 min.

Optogenetic stimulation of SST$^+$ neurons in V1 slice

To elicit SST release from a slice, ChR2(E123T/T159C) expressed in SST$^+$ neurons of V1 was stimulated by 470-nm light pulses (4 to 5 ms in duration), which were delivered to a circular area of 45- to 50-μm radius around the recording cell through a 10× objective lens (Olympus, 0.3 numerical aperture, UMPlanFI, W) using a collimated digital micromirror device coupled light-emitting diode (Polygon400; Mightex Systems, Pleasanton, CA). To examine the effects of SST release on EPSCs on FS neurons, we whole-cell patched FS or RS neurons and monitored sEPSCs in the presence of 100 μM picrotoxin and 1 μM CGP52432 ($GABA_A$ and $GABA_B$ blockers, respectively) in the bath. For stimulation of SST$^+$ INs, 1-s trains of 40-Hz photopulses were applied 16 times every 3.5 s. Effects of stimulation of SST$^+$ neurons were evaluated by measuring the amplitudes and frequencies of sEPSCs 3 min before and after the photostimulation.

In vivo electrophysiology

A head plate was implanted on the dorsal surface of the skull of a mouse and recovered for 1 to 2 days before the recording. Mice were anesthetized by intraperitoneal injection of the urethane dissolved in PBS (2 g per body weight kilogram; Sigma-Aldrich) and anesthetized further by the inhalation of 0.2 to 1% isoflurane. The head was retrained throughout the recording, and the silicon probe (A1x32-Poly2-10 mm-50s-177-CM32 or A1x32-Poly3-10 mm-50-177-CM32, NeuroNexus), was inserted into the V1 by using a microdrive manipulator (Siskiyou). The recording data were acquired by using the RHD 2000-Series Amplifier Evaluation System (Intan Technologies) or the PZ5 Amplifier and the RZ2 Processor (Tucker-Davis Technologies), filtered at 250 to 7500 Hz with a 20-kHz sampling rate. Visual stimulation was generated and given by using Psychtoolbox-3, of which digital output signals were recorded by the amplifier. For the drug treatment, 1 μl of the SST or PBS solutions was carefully applied onto the surface of the dura on top of the V1 where the probe is inserted by using the micropipette. Spikes were isolated by using Klusters (*33*) and analyzed by MATLAB.

Bootstrapping was used for the in vivo recording data to see whether significant firing rate (FR) changes have occurred between two different temporal points or two different orientation points. The number of repetition was set to 5000, and the threshold for the significance was 0.05 to test visual responses and to check the orientation selectivity. Only when the visually evoked firing rates of a unit before and after the PBS treatment were not significantly different, the data were collected for the analysis. OSI was calculated as the following, where θ is the preferred orientation of a unit

$$\mathrm{OSI}\theta = (\mathrm{FR}\theta - \mathrm{mean}(\mathrm{FR}\theta - 90, \mathrm{FR}\theta + 90))/(\mathrm{FR}\theta + \mathrm{mean}(\mathrm{FR}\theta - 90, \mathrm{FR}\theta + 90)); \ \mathrm{mean}(\mathrm{FR}\theta - 90, \mathrm{FR}\theta + 90) > 0.5$$

The normalized FRs of a unit was calculated as the following, where θ is the preferred orientation

$$\mathrm{FRnormalized} = \mathrm{FR}/\mathrm{mean}(\mathrm{FR}\theta - 90, \mathrm{FR}\theta + 90)$$

FR change index between PBS and SST condition was calculated as the following

$$\mathrm{FR\ change\ index}_{\mathrm{PBS\ to\ SST}} = (\mathrm{FR}_{\mathrm{SST}} - \mathrm{FR}_{\mathrm{PBS}})/(\mathrm{FR}_{\mathrm{SST}} + \mathrm{FR}_{\mathrm{PBS}})$$

3D reconstruction of ultrastructures of fluorescence-labeled neurons by SBEM and correlative light-EM

Adult mice (8 to 12 weeks of age) were anesthetized with an overdose of inhalation anesthetic (isoflurane). They were then perfused via the heart, and once fixed, 80-μm-thick, coronal sections of the brain were cut with a vibratome, through the V1 region. These sections were then imaged in L2/3 with confocal microscopy (SP8 STED 3X, Leica). We identified a target area, which had a soma of the red-fluorescent PV$^+$ neuron and the green-fluorescent axon fibers, and reimaged the same area with a custom-built two-photon microscope (*34*). Using a high-power two-photon laser beam, we burnt two vertical and one horizontal line into the fixed tissue around the target area. We then reimaged a series of *z*-sectioned images (300-nm intervals, total 50 to 60 μm along the *z* axis) of the V1 target area to identify the laser marks and the fluorescent signals in the target area using the confocal microscope. We then processed the sample for SBEM imaging of fluorescently labeled axons and soma at the École Polytechnique Fédérale de Lausanne (EPFL) EM core as previously reported (*35*). SBEM imaging was performed in the SEM microscope

(Merlin, Zeiss NTS) fitted with the 3View cutting system (Gatan Inc., Pleasanton, CA, USA) at a resolution of 5.2 nm per pixel in the 2D image plane (a total image size of 6000 × 6000 pixels in one image plane) and 50-nm section thickness. All quantitative analysis of the serial images was carried out using the TrakEM tools (*36*) in the FIJI software (http://fiji.sc/). Three different compartments (soma, axons, and dendrites) were traced across the series of EM images. The measurements of length and volume were made using a NeuroMorph software toolset for 3D analysis of neurite morphology and connectivity (*37*). Synapses were identified by the symmetry of stained pre- and postsynaptic membranes and classified them into type I (asymmetric, excitatory) and type II (symmetric, inhibitory) types. Vesicles inside axons were tracked and classified on the basis of the size and the darkness in the EM images. If the vesicle showed with an appearance of a DCV, then we measured the size and the darkness of the vesicle. Vesicles larger than 45.5 nm in diameter and darker at least three times below than the mean darkness of the same image section were counted as DCVs following the previous literature on the feature of DCVs (*38*).

Statistical analysis

All data were presented as means ± SEM. The "*N*" in figure legends represents "animals" in behavior, and the "*n*" indicates "cells" in single-unit recording experiments. We tested normality of distributions for each dataset using Lilliefors. Bonferroni correction method was used for post hoc multiple comparison tests. Wilcoxon signed-rank test or paired *t* test was used to decide significance in paired comparisons, and Mann-Whitney *U* test or unpaired *t* test was used for unpaired comparisons. The statistical tests used are reported explicitly in the main text or figure legends. Throughout the paper, * indicates $*P < 0.05$, $**P < 0.01$, and $***P < 0.001$. All analyses were performed using custom codes in MATLAB (MathWorks), Excel (Microsoft), and SPSS (IBM).

SUPPLEMENTARY MATERIALS

Supplementary material for this article is available at http://advances.sciencemag.org/cgi/content/full/6/17/eaaz0517/DC1

View/request a protocol for this paper from *Bio-protocol*.

REFERENCES AND NOTES

1. P. Brazeau, W. Vale, R. Burgus, N. Ling, M. Butcher, J. Rivier, R. Guillemin, Hypothalamic polypeptide that inhibits the secretion of immunoreactive pituitary growth hormone. *Science* **179**, 77–79 (1973).
2. J. Epelbaum, Somatostatin in the central nervous system: physiology and pathological modifications. *Prog. Neurobiol.* **27**, 63–100 (1986).
3. H. Adesnik, W. Bruns, H. Taniguchi, Z. J. Huang, M. Scanziani, A neural circuit for spatial summation in visual cortex. *Nature* **490**, 226–231 (2012).
4. H. Makino, T. Komiyama, Learning enhances the relative impact of top-down processing in the visual cortex. *Nat. Neurosci.* **18**, 1116–1122 (2015).
5. D. Kim, H. Jeong, J. Lee, J. W. Ghim, E. S. Her, S. H. Lee, M. W. Jung, Distinct roles of parvalbumin- and somatostatin-expressing interneurons in working memory. *Neuron* **92**, 902–915 (2016).
6. S. C. Baraban, M. K. Tallent, Interneuron Diversity series: Interneuronal neuropeptides--endogenous regulators of neuronal excitability. *Trends Neurosci.* **27**, 135–142 (2004).
7. M. Liguz-Lecznar, J. Urban-Ciecko, M. Kossut, Somatostatin and somatostatin-containing neurons in shaping neuronal activity and plasticity. *Front. Neural Circuits* **10**, 48 (2016).
8. P. Davies, R. Katzman, R. D. Terry, Reduced somatostatin-like immunoreactivity in cerebral cortex from cases of Alzheimer disease and Alzheimer senile dementa. *Nature* **288**, 279–280 (1980).
9. H. M. Morris, T. Hashimoto, D. A. Lewis, Alterations in somatostatin mRNA expression in the dorsolateral prefrontal cortex of subjects with schizophrenia or schizoaffective disorder. *Cereb. Cortex* **18**, 1575–1587 (2008).
10. M. K. Tallent, C. Qiu, Somatostatin: An endogenous antiepileptic. *Mol. Cell. Endocrinol.* **286**, 96–103 (2008).
11. H. Agren, G. Lundqvist, Low levels of somatostatin in human CSF mark depressive episodes. *Psychoneuroendocrinology* **9**, 233–248 (1984).
12. M. Grilli, L. Raiteri, A. Pittaluga, Somatostatin inhibits glutamate release from mouse cerebrocortical nerve endings through presynaptic sst2 receptors linked to the adenylyl cyclase-protein kinase A pathway. *Neuropharmacology* **46**, 388–396 (2004).
13. N. Leresche, E. Asprodini, Z. Emri, D. W. Cope, V. Crunelli, Somatostatin inhibits GABAergic transmission in the sensory thalamus via presynaptic receptors. *Neuroscience* **98**, 513–522 (2000).
14. V. G. Lopez-Huerta, F. Tecuapetla, J. N. Guzman, J. Bargas, E. Galarraga, Presynaptic modulation by somatostatin in the neostriatum. *Neurochem. Res.* **33**, 1452–1458 (2008).
15. J. R. Mancillas, G. R. Siggins, F. E. Bloom, Somatostatin selectively enhances acetylcholine-induced excitations in rat hippocampus and cortex. *Proc. Natl. Acad. Sci. U.S.A.* **83**, 7518–7521 (1986).
16. J. R. Delfs, M. A. Dichter, Effects of somatostatin on mammalian cortical neurons in culture: Physiological actions and unusual dose response characteristics. *J. Neurosci.* **3**, 1176–1188 (1983).
17. C. Videau, U. Hochgeschwender, H. J. Kreienkamp, M. B. Brennan, C. Viollet, D. Richter, J. Epelbaum, Characterisation of [125I]-Tyr0DTrp8-somatostatin binding in sst1- to sst4- and SRIF-gene-invalidated mouse brain. *Naunyn Schmiedebergs Arch. Pharmacol.* **367**, 562–571 (2003).
18. C. K. Pfeffer, M. Xue, M. He, Z. J. Huang, M. Scanziani, Inhibition of inhibition in visual cortex: the logic of connections between molecularly distinct interneurons. *Nat. Neurosci.* **16**, 1068–1076 (2013).
19. S.-H. Lee, A. C. Kwan, S. Zhang, V. Phoumthipphavong, J. G. Flannery, S. C. Masmanidis, H. Taniguchi, Z. J. Huang, F. Zhang, E. S. Boyden, K. Deisseroth, Y. Dan, Activation of specific interneurons improves V1 feature selectivity and visual perception. *Nature* **488**, 379–383 (2012).
20. B. V. Atallah, W. Bruns, M. Carandini, M. Scanziani, Parvalbumin-expressing interneurons linearly transform cortical responses to visual stimuli. *Neuron* **73**, 159–170 (2012).
21. N. R. Wilson, C. A. Runyan, F. L. Wang, M. Sur, Division and subtraction by distinct cortical inhibitory networks in vivo. *Nature* **488**, 343–348 (2012).
22. S. H. Lee, A. C. Kwan, Y. Dan, Interneuron subtypes and orientation tuning. *Nature* **508**, E1–E2 (2014).
23. D. Shakiryanova, A. Tully, R. S. Hewes, D. L. Deitcher, E. S. Levitan, Activity-dependent liberation of synaptic neuropeptide vesicles. *Nat. Neurosci.* **8**, 173–178 (2005).
24. L. de Lecea, J. R. Criado, Ó. Prospero-Garcia, K. M. Gautvik, P. Schweitzer, P. E. Danielson, C. L. M. Dunlop, G. R. Siggins, S. J. Henriksen, J. G. Sutcliffe, A cortical neuropeptide with neuronal depressant and sleep-modulating properties. *Nature* **381**, 242–245 (1996).
25. B. Tasic, Z. Yao, L. T. Graybuck, K. A. Smith, T. N. Nguyen, D. Bertagnolli, J. Goldy, E. Garren, M. N. Economo, S. Viswanathan, O. Penn, T. Bakken, V. Menon, J. Miller, O. Fong, K. E. Hirokawa, K. Lathia, C. Rimorin, M. Tieu, R. Larsen, T. Casper, E. Barkan, M. Kroll, S. Parry, N. V. Shapovalova, D. Hirschstein, J. Pendergraft, H. A. Sullivan, T. K. Kim, A. Szafer, N. Dee, P. Groblewski, I. Wickersham, A. Cetin, J. A. Harris, B. P. Levi, S. M. Sunkin, L. Madisen, T. L. Daigle, L. Looger, A. Bernard, J. Phillips, E. Lein, M. Hawrylycz, K. Svoboda, A. R. Jones, C. Koch, H. Zeng, Shared and distinct transcriptomic cell types across neocortical areas. *Nature* **563**, 72–78 (2018).
26. R. L. Adlington, K. R. Laws, T. M. Gale, Visual processing in Alzheimer's disease: Surface detail and colour fail to aid object identification. *Neuropsychologia* **47**, 2574–2583 (2009).
27. Y. Gonchar, S. Turney, J. L. Price, A. Burkhalter, Axo-axonic synapses formed by somatostatin-expressing GABAergic neurons in rat and monkey visual cortex. *J. Comp. Neurol.* **443**, 1–14 (2002).
28. G. A. Hicks, W. Feniuk, P. P. Humphrey, Outward current produced by somatostatin (SRIF) in rat anterior cingulate pyramidal cells in vitro. *Br. J. Pharmacol.* **124**, 252–258 (1998).
29. P. Dournaud, Y. Z. Gu, A. Schonbrunn, J. Mazella, G. S. Tannenbaum, A. Beaudet, Localization of the somatostatin receptor SST_{2A} in rat brain using a specific anti-peptide antibody. *J. Neurosci.* **16**, 4468–4478 (1996).
30. M. Schindler, L. A. Sellers, P. P. Humphrey, P. C. Emson, Immunohistochemical localization of the somatostatin $SST_{2(A)}$ receptor in the rat brain and spinal cord. *Neuroscience* **76**, 225–240 (1997).
31. S. Schulz, M. Händel, M. Schreff, H. Schmidt, V. Höllt, Localization of five somatostatin receptors in the rat central nervous system using subtype-specific antibodies. *J. Physiol. Paris* **94**, 259–264 (2000).
32. C. Bodenant, P. Leroux, B. J. Gonzalez, H. Vaudry, Transient expression of somatostatin receptors in the rat visual system during development. *Neuroscience* **41**, 595–606 (1991).
33. L. Hazan, M. Zugaro, G. Buzsáki, Klusters, NeuroScope, NDManager: A free software suite for neurophysiological data processing and visualization. *J. Neurosci. Methods* **155**, 207–216 (2006).

34. M. Avermann, C. Tomm, C. Mateo, W. Gerstner, C. C. Petersen, Microcircuits of excitatory and inhibitory neurons in layer 2/3 of mouse barrel cortex. *J. Neurophysiol.* **107**, 3116–3134 (2012).
35. C. Maclachlan, D. A. Sahlender, S. Hayashi, Z. Molnár, G. Knott, Block face scanning electron microscopy of fluorescently labeled axons without using near infra-red branding. *Front. Neuroanat.* **12**, 88 (2018).
36. A. Cardona, S. Saalfeld, J. Schindelin, I. Arganda-Carreras, S. Preibisch, M. Longair, P. Tomancak, V. Hartenstein, R. J. Douglas, TrakEM2 software for neural circuit reconstruction. *PLOS ONE* **7**, e38011 (2012).
37. A. Jorstad, J. Blanc, G. Knott, NeuroMorph: A software toolset for 3D analysis of neurite morphology and connectivity. *Front. Neuroanat.* **12**, 59 (2018).
38. M. Hammarlund, S. Watanabe, K. Schuske, E. M. Jorgensen, CAPS and syntaxin dock dense core vesicles to the plasma membrane in neurons. *J. Cell Biol.* **180**, 483–491 (2008).
39. Z. V. Guo, N. Li, E. Ophir, D. Gutnisky, J. T. Ting, G. Feng, K. Svoboda, Flow of cortical activity underlying a tactile decision in mice. *Neuron* **81**, 179–194 (2014).
40. P. Le Merre, V. Esmaeili, E. Charrière, K. Galan, P. A. Salin, C. C. H. Petersen, S. Crochet, Reward-based learning drives rapid sensory signals in medial prefrontal cortex and dorsal hippocampus necessary for goal-directed behavior. *Neuron* **97**, 83–91.e5 (2018).

Acknowledgments: We thank M. Andermann, A. Magnusson, and S. Lejion for helpful discussions. **Funding:** This work was supported by grants to Seung-Hee Lee from the National Research Foundation of Korea funded by the Ministry of Science & ICT (NRF-2016K2A9A2A12003799, 2017R1A2B3008270, 2016M3A6A6930773, 2017M3C7A1030798, and 2018R1A4A1025616) and from ETRI funded by the Korean government (19ZS150). A Global Ph.D. fellowship supported Y.-H.S., and a TJ Park Science fellowship supported K.K. **Author contributions:** Seung-Hee Lee conceived and supervised all experiments and wrote the manuscript. Y.-H.S. and Y.-S.H. analyzed data and wrote the manuscript. Y.-H.S., Y.-S.H., and K.K. performed behavior experiments. Y.-H.S., K.K., and J.-H.K. performed in vivo recording experiments. H.-R.L., K.K., and Suk-Ho Lee performed in vitro patch-clamp recordings. Y.-S.H., C.M., A.D., C.C.H.P., and G.K. performed the 3D EM tracing experiment. M.W.J. supported building the T-maze behavior setup. **Competing interests:** The authors declare that they have no competing interests. **Data and materials availability:** The licenses for Fiji, MATLAB, SPSS, and Excel are commercially available, NeuroMorph can be freely downloaded at https://github.com/NeuroMorph-EPFL/NeuroMorph, and the Klusters software can be freely downloaded at http://neurosuite.sourceforge.net/. All data needed to evaluate the conclusions in the paper are present in the paper and/or the Supplementary Materials. Additional data related to this paper may be requested from the authors. Further requests for custom scripts and data used in this study can be directed to the corresponding author (shlee1@kaist.ac.kr).

Submitted 7 August 2019
Accepted 3 February 2020
Published 22 April 2020
10.1126/sciadv.aaz0517

Citation: Y.-H. Song, Y.-S. Hwang, K. Kim, H.-R. Lee, J.-H. Kim, C. Maclachlan, A. Dubois, M. W. Jung, C. C. H. Petersen, G. Knott, S.-H. Lee, S.-H. Lee, Somatostatin enhances visual processing and perception by suppressing excitatory inputs to parvalbumin-positive interneurons in V1. *Sci. Adv.* **6**, eaaz0517 (2020).